http://www.jstage.jst.go.jp/browse/biophysics

BIOPHYSICS

Vol. 9, pp. 173–181 (2013)
doi: 10.2142/biophysics.9.173

# The C-terminal periplasmic domain of MotB is responsible for load-dependent control of the number of stators of the bacterial flagellar motor

David J. Castillo[1], Shuichi Nakamura[2], Yusuke V. Morimoto[1,3], Yong-Suk Che[4], Nobunori Kami-ike[1], Seishi Kudo[2], Tohru Minamino[1] and Keiichi Namba[1,3]

[1]*Graduate School of Frontier Biosciences, Osaka University, 1-3 Yamadaoka, Suita, Osaka 565-0871, Japan*
[2]*Department of Applied Physics, Tohoku University, 6-6-05 Aoba, Aramakiaza, Aoba-ku, Sendai, Miyagi 980-8579, Japan*
[3]*Quantitative Biology Center, RIKEN, 6-2-3 Furuedai, Suita, Osaka 565-0874, Japan*
[4]*Department of Frontier Bioscience, Hosei University, 3-7-2 Kajino-cho, Koganei, Tokyo 184-8584, Japan*

Received October 23, 2013; accepted December 7, 2013

**The bacterial flagellar motor is made of a rotor and stators. In *Salmonella* it is thought that about a dozen MotA/B complexes are anchored to the peptidoglycan layer around the motor through the C-terminal peptidoglycan-binding domain of MotB to become active stators as well as proton channels. MotB consists of 309 residues, forming a single transmembrane helix (30–50), a stalk (51–100) and a C-terminal peptidoglycan-binding domain (101–309). Although the stalk is dispensable for torque generation by the motor, it is required for efficient motor performance. Residues 51 to 72 prevent premature proton leakage through the proton channel prior to stator assembly into the motor. However, the role of residues 72–100 remains unknown. Here, we analyzed the torque-speed relationship of the MotB(Δ72–100) motor. At a low speed near stall, this mutant motor produced torque at the wild-type level. Unlike the wild-type motor, however, torque dropped off drastically by slight decrease in external load and then showed a slow exponential decay over a wide range of load by its further reduction. Since it is known that the stator is a mechanosensor and that the number of active stators changes in a load-dependent manner, we interpreted this unusual torque-speed relationship as anomaly in load-dependent control of the number of active stators. The results suggest that residues 72–100 of MotB is required for proper load-dependent control of the number of active stators around the rotor.**

**Key words:** *Salmonella*, torque generation, torque-speed curve, mechanosensor, proton channel

The bacterial flagellar motor is a rotary nanomachine powered by the electrochemical potential gradient of protons or sodium ions across the cytoplasmic membrane. The flagellar motor of *Salmonella enterica* serovar Typhimurium (thereafter referred to *Salmonella*) consists of a rotor and a dozen stators. The rotor consists of four proteins, FliF, FliG, FliM, and FliN. Twenty six copies of FliF form the MS ring spanning the cytoplasmic membrane, and its diameter is 27 nm. FliG, FliM, and FliN form the C ring with a diameter of 44 nm on the cytoplasmic face of the MS ring. FliG, FliM, and FliN also act as a switch complex, enabling the motor to spin in both counterclockwise and clockwise directions. The stator consists of four copies of MotA and two copies of MotB and acts as a proton channel to couple proton flow through the channel with torque generation. The stator is postulated to be anchored to the peptidoglycan (PG) layer through a well-conserved peptidoglycan binding

*D. J. Castillo and S. Nakamura contributed equally to this work.
Corresponding authors: Tohru Minamino, Graduate School of Frontier Biosciences, Osaka University, 1-3 Yamadaoka, Suita, Osaka 565-0871, Japan. e-mail: tohru@fbs.osaka-u.ac.jp;
Keiichi Namba, Graduate School of Frontier Biosciences, Osaka University, 1-3 Yamadaoka, Suita, Osaka 565-0871, Japan.
e-mail: keiichi@fbs.osaka-u.ac.jp

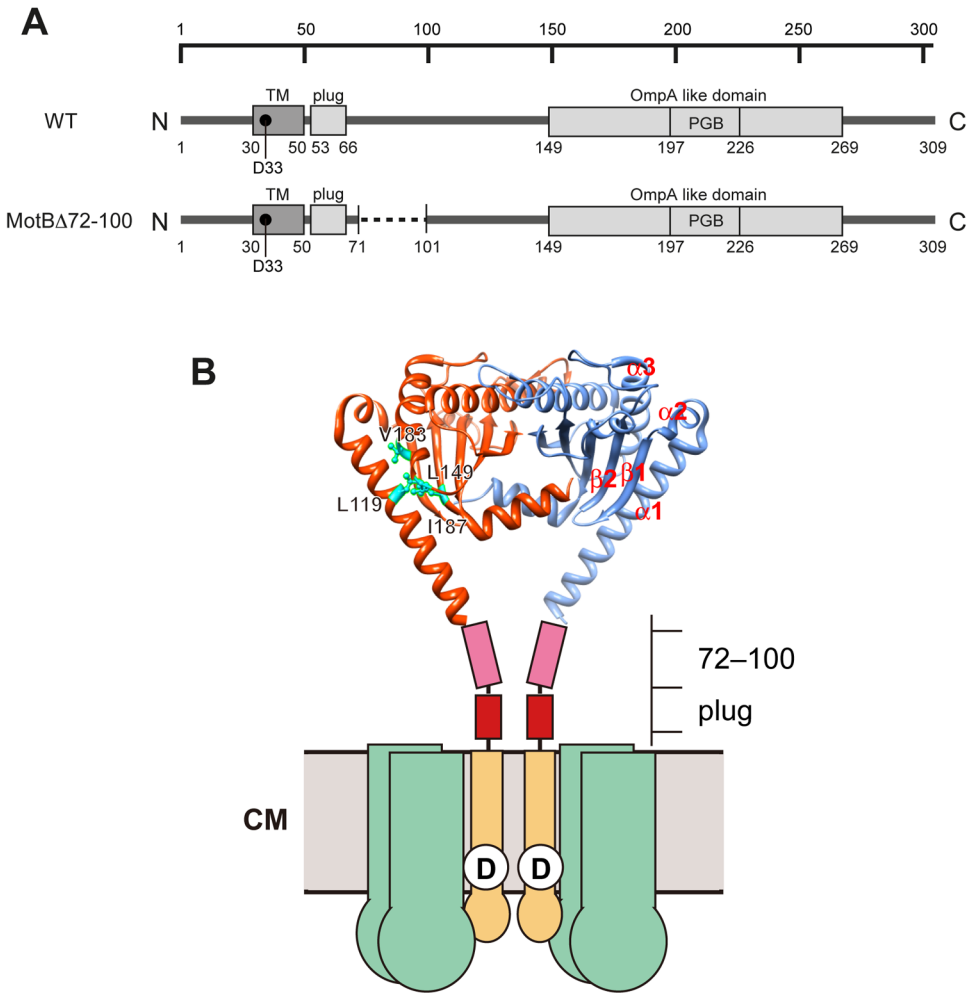


**Figure 1** Primary structure of MotB and MotB(Δ72–100). (A) *Salmonella* MotB contains 309 amino acids and has a single transmembrane domain ('TM', residues 30–50) and a periplasmic region including an OmpA-like domain (residues 149–269) with a putative peptidoglycan-binding (PGB) motif (residues 197–226). MotB-Asp33 is a proton-binding site. Residues 53–66 works as a plug of the MotA/B proton channel to prevent premature proton leakage prior to stator assembly around the motor. (B) Cα ribbon representation of *Salmonella* $MotB_C$ dimer in the crystal (PDB ID: 2ZVY) with the proton channel domain of the MotA/B complex and a stalk domain of MotB (residues 51–100) connecting these two. The two subunits are shown in blue and orange. The stator consists of four copies of MotA and two copies of MotB. The $MotB_C$ dimers are connected to MotB-TMs (yellow box) through a linker region containing the plug segment (residues 53–66) and residues 72–100. MotB-TM forms a proton channel along with MotA-TM3 and MotA-TM4. Leu119 in helix α1 shows hydrophobic interactions with Leu149 in strand β2 and Val183 and Ile187 after helix α3.

(PGB) motif of MotB in its C-terminal periplasmic region[1–4]. Highly conserved charged residues at the stator-rotor interface are required not only for torque generation[5] but also for stator assembly around the rotor[6,7].

MotA is a 295-residue protein, possessing four transmembrane (TM) helices, connected with two periplasmic loops and a large cytoplasmic loop between TM-2 and TM-3. MotB consists of 309 residues, containing a small N-terminal cytoplasmic segment (residue 1–29), a single TM helix (residue 30–50) and a large C-terminal periplasmic domain (residue 51–309; $MotB_C$) (Fig. 1A)[1–4]. MotB-TM forms a proton channel with the TM-3 and TM-4 helices of MotA[8–10]. Asp33 of *Salmonella* MotB, which is a highly conserved aspartic residue among MotB orthologues, is located at the proximal end of MotB-TM and is critical for proton translocation through the channel (Fig. 1B)[11]. MotA-Pro173, which is highly conserved among MotA orthologues, is in close proximity to MotB-Asp33 and facilitates the conformational dynamics of the stator for rapid proton translocation and torque generation cycle[12,13].

$MotB_C$ forms a homo-dimer, and its dimerization is essential for MotB function[14]. A well-conserved PGB motif in $MotB_C$ shows a significant sequence similarity to OmpA-like proteins (Fig. 1A)[15]. The crystal structures of $MotB_C$ derived from *Helicobacter pilori*[16] and *Salmonella*[17] have been solved by X-ray crystallography, and the core of the domain has a typical OmpA-like structure, which adopts a β-α-β-α-β-β fold (Fig. 1B). $MotB_C$ is required not only for

proper anchoring of the stator to its binding-site on the motor[18] but also for proper alignment of the stator relative to the rotor[19]. Rapid exchange of stators occurs between the motor and the cytoplasmic membrane pool, suggesting that the interaction between the stator and the PG layer is highly dynamic during motor rotation[20–22]. Recently, it has been shown that the number of stators driving the motor changes depending on external load, being much less at very low load than that at high load[23,24]. Furthermore, it has been reported that the MotA/B complex is a load-sensitive proton channel that efficiently couples proton translocation with the conformational changes for torque generation[25]. These observations suggest that the stator is a mechanosensor to control the power-load balance of the motor function in response to load change but it remains unknown how they do.

Residues 51–100 in MotB form a stalk connecting the PGB domain to MotB-TM. *Salmonella* MotB missing the entire stalk still retains the ability to act as the stator element to a considerable degree although not to the wild-type level. This indicates that the stalk contributes to efficient motor performance although it is dispensable for the basic stator function for torque generation[17,26]. It has been shown that deletion of residues from Pro53 to Pro66 of *Salmonella* MotB just after the TM segment (Pro52 to Pro65 in *E. coli* MotB) causes massive proton flow through the MotA/B proton channel complexes in the membrane pool, suggesting that the deleted region acts as a plug for the proton channel to suppress undesirable proton leakage into the cytoplasm when the MotA/B complex is not assembled into the motor[27,28]. In contrast, little is known about the role of the rest of the stalk region.

Here, we investigated the torque-speed relationship of the flagellar motor of the *Salmonella motB*(Δ72–100) mutant (thereafter referred to the MotB(Δ72–100) motor) by bead assays. We show that torque produced by fully-induced MotB(Δ72–100) mutant motor is at the wild-type level when external load is extremely high but drops off drastically by slight decrease in external load, suggesting anomaly in load-dependent control of the number of active stators. We will discuss the role of residues 72–100 of MotB in flagellar motor rotation.

## Results

### Effect of deletion of residues 72 to 100 of MotB on the torque-speed relationship

To investigate the effect of in-frame deletion of residues 72 to 100 of MotB on torque generation under a wide range of external load conditions, we constructed a pBAD24-based plasmid encoding the MotA/B(Δ72–100) complex under control of the arabinose pBAD promoter and analyzed the swimming motility of *Salmonella* cells expressing MotA/B(Δ72–100) in liquid media under a phase contrast microscope (Fig. 2). Quantitative immunoblotting with polyclonal anti-MotB antibody revealed that the expression level of MotB(Δ72–

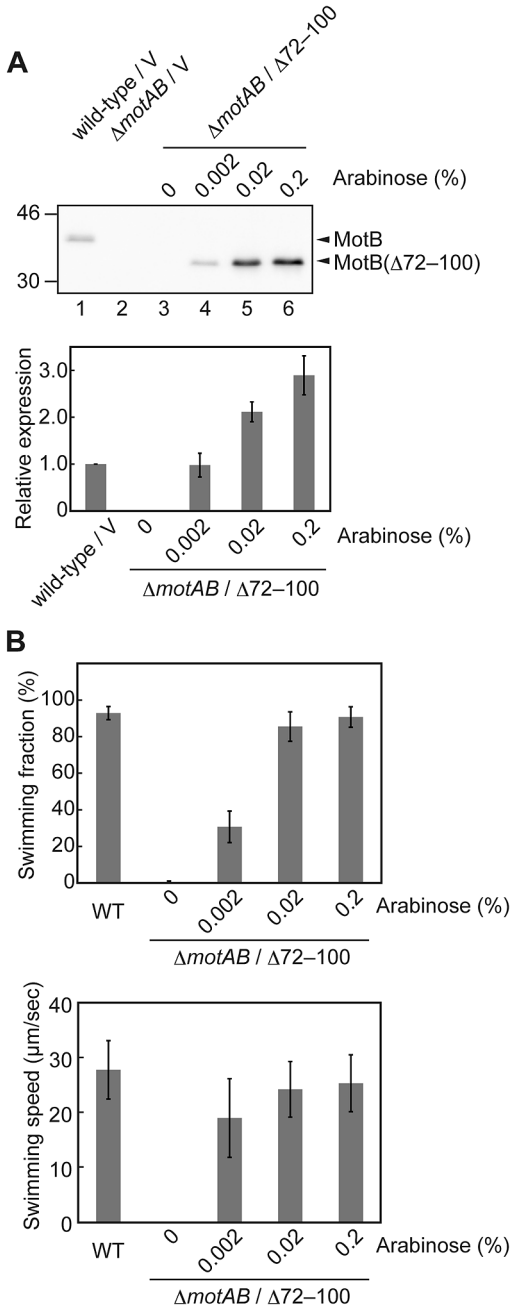


**Figure 2** Swimming motility of the *Salmonella motB*(Δ72–100) deletion mutant in liquid media. (A) Immunoblotting, using polyclonal anti-MotB antibody, of whole-cell proteins prepared from SJW1103 (wild type) carrying pBAD24 (V), and SJW2241(Δ*motA-motB*) carrying pBAD24 (V) or pDC1 (MotA/B(Δ72–100)) were incubated at 30°C for 5 h in LB with 0%, 0.002%, 0.02%, 0.2% arabinose. Arrowhead indicates the positions of MotB and MotB(Δ72–100). Lower panel shows the relative expression levels of MotB and MotB(Δ72–100). The integrated density of each band are normalized to that of wild-type MotB expressed from the chromosome (lane 1). These data are the average of five independent experiments. Error bars show standard deviations. (B) Free-swimming fraction and speed of SJW1103 (WT) and SJW2241(Δ*motAB*) carrying pDC1 (MotA/B(Δ72–100)). Swimming fraction is the number fraction of swimming cells. Swimming speed is the average of more than 30 cells, and vertical lines are standard deviations. Measurements were performed at ca. 23°C under a phase contrast microscope.

100) induced by addition of 0.002% arabinose was almost the same as that of MotB expressed from the chromosome of wild-type cells (Fig. 2A, lanes 1 and 4) and increased by about two and three fold when 0.02% and 0.2% arabinose was added, respectively (lanes 5 and 6). About 70% of the cells expressing the MotA/B(Δ72–100) complex at the wild-type level were non-motile (Fig. 2B). However, the mutant cells became almost fully motile at two-fold higher expression level, with their swimming speed reaching about 90% of the wild-type level (Fig. 2B). These results suggest that deletion of residues 72–100 within $MotB_C$ reduces the binding affinity of the stators for their binding sites on the motor but does not significantly affect the rotor-stator interactions for torque generation.

We then measured the rotation rates of beads attached to partially sheared, sticky filaments of fully induced MotB(Δ72–100) motors. We used the MM3076iC strain harboring pBAD24 (vector control; thereafter referred to the wild-type motor) as the wild-type control. Figure 3 shows typical examples of bead rotation attached to the wild-type (Fig. 3A, B, C) and MotB(Δ72–100) (Fig. 3D, E, F) motors under three different external load conditions. To evaluate the speed stability, we calculated the ratio of standard deviation ($\sigma_\omega$) and average of the rotation speed ($<\omega>$) (Table 1) as described by Muramoto *et al*[32]. The values of $\sigma_\omega/<\omega>$ of these two motors were almost constant over a wide range of external load (Table 1), indicating that these two motors can spin stably.

Figure 4 shows torque-speed curves of the wild-type and MotB(Δ72–100) motors, for which data are listed in Table 1.

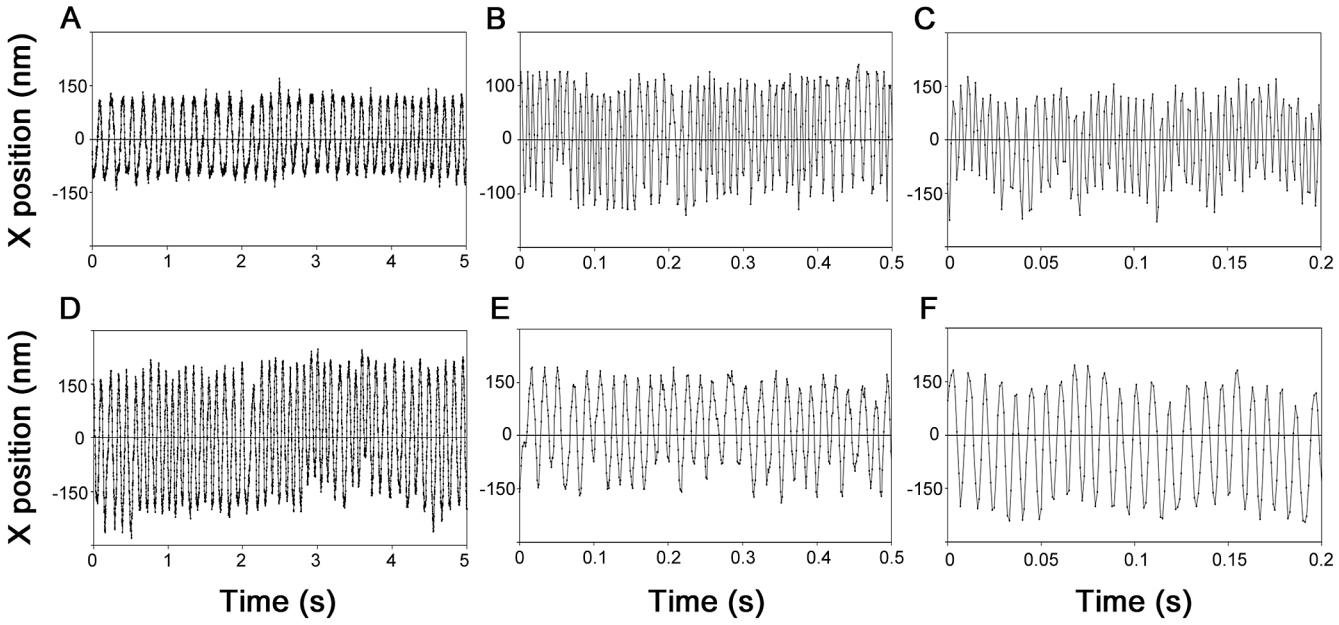


**Figure 3** Rotation measurements of beads attached to the wild-type and MotB(Δ72–100) motors by bead assays. A, B and C are data sets of MM3076iC (Δ*cheA-cheZ fliC*(Δ204–292)) carrying pBAD24, and D, E and F are data sets of YSC2123 (Δ*motA-motB* Δ*cheY fliC*(Δ204–292)) carrying pDC1 (MotA/B(Δ72–100)). A and D, B and E, and C and F were obtained using 1.0-μm beads in the absence of Ficoll, 0.5-μm beads in the presence of 6% Ficoll, and 60-nm gold nanoparticles in the absence of Ficoll, respectively.

**Table 1** Rotation rates and torques of the wild-type motor and in-frame-deletion motors

| | Bead | 1.0 μm | 1.0 μm | 0.5 μm | 0.5 μm | 0.5 μm | 60 nm |
|---|---|---|---|---|---|---|---|
| | Ficoll | 12% | – | 6% | 3% | – | – |
| WT | Rotation rate (Hz) | 9±1 | 57±9 | 119±24 | 179±34 | 210±36 | 252±44 |
| | Torque (pN nm) | 1755±252 | 1636±260 | 1341±213 | 1240±212 | 883±137 | 506±87 |
| | $\sigma_\omega/<\omega>$ | 0.17 | 0.13 | 0.17 | 0.16 | 0.18 | 0.21 |
| | *n* | 17 | 17 | 13 | 11 | 10 | 10 |
| MotB(Δ72-100) | Rotation rate (Hz) | 11±2 | 51±11 | 62±18 | 83±27 | 100±25 | 154±28 |
| | Torque (pN nm) | 2174±441 | 1432±297 | 754±206** | 623±207** | 444±136** | 311±54** |
| | $\sigma_\omega/<\omega>$ | 0.12 | 0.14 | 0.15 | 0.16 | 0.15 | 0.21 |
| | *n* | 16 | 17 | 14 | 13 | 14 | 9 |

Values with asterisks (**) exhibited statistically significant differences ($P<0.001$) compared with the wild-type motor (WT).

The value of $\sigma_\omega/<\omega>$ is average of *n* motors in each condition. The value of $\sigma_\omega/<\omega>$ for each motors was calculated as described in Materials and Methods.

The torque-speed curve of the flagellar motor consists of two regimes: a high-load, low-speed regime and a low-load, high-speed regime[33–37]. In the high-load, low-speed regime, the speed of the motor is proportional to the number of stators, whereas in the low-load, high-speed regime, one stator unit can spin the motor at the maximum speed[23,24,38,39]. In agreement with previous reports[33–37], the wild-type motor showed a typical torque-speed curve with a gradual decrease in high-load regime and a rapid drop in low-load regime (Fig. 4 symbols in black). Torque decreased gradually from about 1,760 pN nm at around 10 Hz (closed circle; 1.0-μm bead in 12% Ficoll) up to a point called the knee at which torque was 1,240 pN nm at around 180 Hz (open triangle; 0.5-μm bead in 3% Ficoll) and then dropped rapidly to 510 pN nm at around 250 Hz (open square; 60-nm bead in water). The maximum rotation speed estimated by linear extrapolation of the torque-speed curve to zero load was approximately 300 Hz.

In contrast, fully induced MotB(Δ72–100) motor showed an unusual torque-speed curve with a rapid drop in high-load regime and a slow decrease in low-load regime (Fig. 4 symbols in red). Torque at extremely high load (1.0-μm bead in 12% Ficoll) was about 2,170 pN nm at around 10 Hz (closed circle), which is even higher than that of the wild-type. But then torque decreased rapidly to 1,430 pN nm at around 50 Hz (open circle; 1.0-μm bead in water) and further down to 750 pN nm at around 60 Hz (closed triangle; 0.5-μm bead in 6% Ficoll) by slight reduction in load. Then torque reduction by further decrease in load was gradual, showing a slow exponential decrease from 750 to 310 pN nm over a speed range from 60 to 160 Hz. The maximum rotation speed estimated by simple linear extrapolation of the torque-speed curve to zero load was approximately 300 Hz, nearly the same as that of the wild-type motor, although this may be an overestimation because the torque-speed curve of the mutant motor would also have the knee point and a rapid drop off just as that of the wild-type motor in the extremely low load region that we could not observe in the present study.

The rotation rate of the proton-driven flagellar motor is known to be proportional to PMF across the cytoplasmic membrane[29], raising the possibility that deletion of residues 72–100 of MotB could have changed PMF, thereby affecting the torque-speed relationship. Because PMF consists of two components: the electric potential difference ($\Delta\psi$) and the proton concentration difference ($\Delta$pH), we separately measured $\Delta\psi$ and intracellular pH of the wild-type cells and the mutant cells expressing MotA/B(Δ72–100) at an external pH value of 7.0 by using tetramethylrhodamine methyl ester[30] and a ratiometric pH indicator protein, pHluorin[31], respectively, and then calculated total PMF. The PMF of the wild-type and mutant cell was −117 mV and −122 mV, respectively, indicating that the 3-fold higher expression of the MotA/B(Δ72–100) complex does not affect PMF at all.

Since PMF was not affected by the over-expression of the MotA/B(Δ72–100) complex, each stator unit of the MotB(Δ72–100) motor must be producing slightly higher torque than that of the wild-type at extremely high load. Deletion of residues 72–100 of MotB may have strengthened the stator-rotor interactions involved in torque generation or improved energy coupling efficiency at extremely high load. However, the performance of the mutant motor was markedly deteriorated by a small reduction in load either by weakened stator-rotor interactions or reduced energy coupling efficiency. Then again, the mutant motor appears to rotate as fast as the wild-type motor at extremely low load, suggesting that the rate of mechanochemical reaction cycle for torque generation is not affected so much by the deletion of residues 72–100. We inferred from these load-dependent changes in the motor performance that mechanosensitive regulation of the attachment of stators to the motor is affected by the deletion.

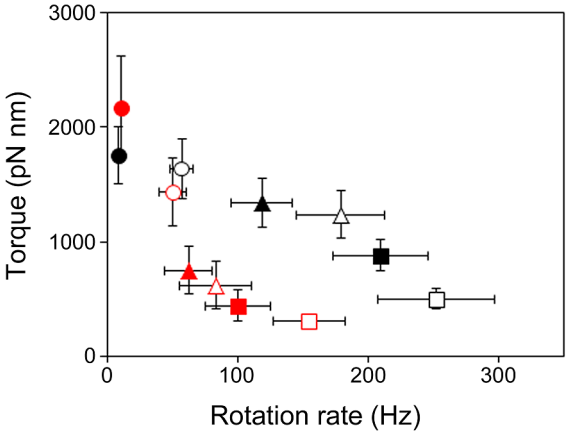


**Figure 4** Torque-speed relationships of the wild-type and MotB(Δ72–100) motors. Measurements were carried out using polystyrene beads with diameters of 1.0 and 0.5 μm and a gold particle with a diameter of 60 nm in motility media (pH 7.0) with or without Ficoll: 1.0 μm in 12% Ficoll (closed circles), 1.0 μm in 0% Ficoll (open circles), 0.5 μm in 6% Ficoll (closed triangles), 0.5 μm in 3% Ficoll (open triangles), 0.5 μm in 0% Ficoll (closed squares) and 60 nm in 0% Ficoll (open squares). Probes were attached to the sticky filaments of MM3076iC cells carrying pBAD24 (black symbols) and YSC2123 cells carrying pDC01 (red symbols). Error bars are standard deviations. Data are listed in Table 1.

## Estimation of the number of stators

About a dozen stators are installed at most into the flagellar motor[40]. It has been shown, however, that the flagellar motor is also a mechanosensor and dynamically changes the number of stators driving the motor in response to changes in external load[23,24]. The peculiar torque-speed curve of fully induced MotB(Δ72–100) motor, showing an early drop off in relatively high load regime and sustained low torque over a wide range of load from medium to low load up to near maximum speed (Fig. 4), raised the possibility that the deletion of residues 72–100 considerably affects the load-dependent regulatory mechanism of the number of active

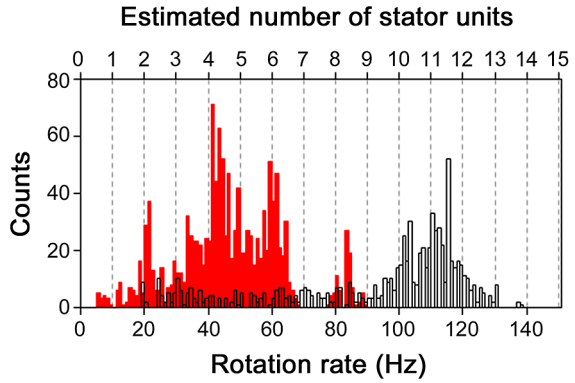


**Figure 5** Speed histograms of the wild-type and MotB(Δ72–100) motors. Rotation rates of single wild-type (open black bar) and MotB(Δ72–100) (filled red bar) motors labeled with 0.5-μm beads in the presence of 6% Ficoll were determined from power spectra using 1.0-sec data windows (1024 points) at an interval of 0.1 sec. The number labels above the data represent the units corresponding to multiples of 10 Hz. The peaks of rotation rates correspond to these units, indicating the presence of different numbers of stators driving the motor.

stators around the rotor. To estimate the number of stators in the MotB(Δ72–100) motor, we made a histogram of rotation rates that were determined from power spectra, each calculated from a 1-sec long data window shifted every 0.1 sec over 10-sec data records obtained from single motors labeled with 0.5-μm beads in 6% Ficoll solution with a sampling rate of 1 kHz. The data corresponds to those represented by the closed triangles in Figure 4. Figure 5 shows two speed histograms, one for the wild-type (black) and the other for the MotB(Δ72–100) motor (red). The rotation rates of the wild-type motors were mostly distributed over a relatively narrow range from 95 to 125 Hz with a long tail toward low speed (20 Hz) and showed two distinct peaks at 103 and 113 Hz with an interval of about 10 Hz (Fig. 5). In contrast, the MotB(Δ72–100) motor rotated at speeds ranging from 5 to 90 Hz and showed several distinct peaks at around 20, 30, 40, 50, 60 and 80 Hz. Because the motor speed can be proportional to the number of active stators in high-load, low-speed regime[38–40], the number of stators estimated from these measurements is 10 to 11 for the wild-type and 2 to 6 for the MotB(Δ72–100) motors. This result indicates the involvement of residues 72–100 in the mechanosensitive regulation of the number of active stators.

## Discussion

It has been reported that a few stators spin the motor at low loads and that 6–11 stators drive the same motor at high loads[23,24]. This suggests that the flagellar motor control the number of stators in the motor in response to changes in external load. It has also been shown that the stator acts as a load-sensitive proton channel that efficiently couples proton translocation with torque generation and that Asp33 of MotB is critical for this coordinated proton translocation[25]. However, it remained unknown how the motor regulates the assembly and disassembly of the stators in response to the load change. Here, we carried out high-resolution bead assays over a wide rage of external load to analyze the torque-speed relationship of the MotB(Δ72–100) mutant motor lacking resides 72 to 100, which forms part of the stalk connecting the transmembrane helix to the PGB domain of the MotA/B complex (Fig. 1B). When MotB(Δ72–100) was expressed at the wild-type level, 70% of the cells were non-motile. However, an increment in the expression level of MotB(Δ72–100) by 2-fold allowed most of the cells to become motile at about 90% of the wild-type speed (Fig. 2). This indicates that deletion of residues 72–100 in MotB causes 2-fold reduction in the efficiency of stator assembly into the motor. Because $MotB_C$ is responsible for stable anchoring of the stator to its binding-site on the motor[18], we suggest that the shortening of the stalk by the deletion reduces the binding affinity of the stator by 2-fold. At low speed near stall, fully induced MotB(Δ72–100) motor produced torque even higher than the wild-type level albeit slightly (Fig. 4), indicating that the deletion does not affect the toque generation step by stator-rotor interactions coupled with proton translocation through the channel of the stator. In contrast, as motor speed increased, torque produced by the MotB(Δ72–100) motor dropped off at much higher load than that of the wild-type motor (Fig. 4). The number of stators estimated from the histogram of rotation rates generated from power spectra of temporal records of bead rotation at medium load was 10 to 11 for the wild-type and 2 to 6 for the MotB(Δ72–100) motors (Fig. 5). These results imply that the load-sensing mechanism regulating the number of active stators is somehow impaired by the reduced affinity of the mutant stator for the motor and that the number of active stators dropped off drastically by a small amount of reduction in external load.

The unusual torque-speed relationship of the MotB(Δ72–100) mutant motor observed in the present study can be explained by load-dependent changes in the number of active stators as shown in Figure 6, in which steady-state torque-speed curves of the MotB(Δ72–100) motors having different number of stators driving the motor are presented. The six load lines corresponding to different bead sizes and viscosities of motility media used in our experiments are also presented by dotted lines ($L1$ to $L6$). From the speed histograms of the wild-type and MotB(Δ72–100) motors operating at external load $L_4$ (Fig. 5), the number of stators of the wild-type and MotB(Δ72–100) motors were estimated to be 11 and 4, respectively. Therefore we assumed that the MotB(Δ72–100) motor contained 11 stators at extremely high load $L_6$ and that the number of stators decreased to 8 at $L_5$, 4 at $L_4$, 3–4 at $L_3$, 2–3 at $L_2$, and 2 at $L_1$ (Fig. 6). This interpretation of the observed data suggests that residues 72 to 100 of MotB is required for proper control of the load-dependent installation of the stators and that the deletion induces the dissociation of stators from the motor at much

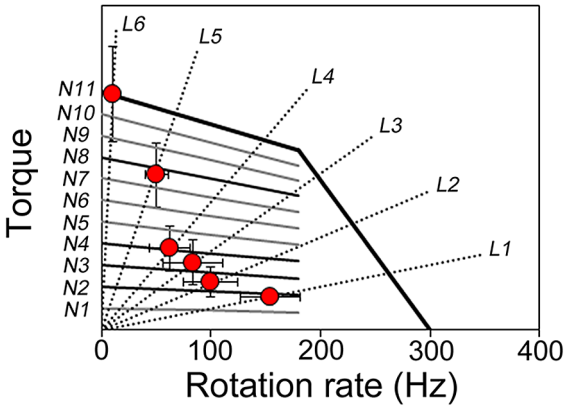


**Figure 6** Qualitative interpretation of the torque-speed curves of the MotB(Δ72–100) motor. Load lines are indicated with dotted lines ($L_1$<$L_2$<$L_3$<$L_4$<$L_5$<$L_6$). Torque-speed curves with different number of stator units are indicated ($N_1$–$N_{11}$). Points where the load lines cross thick solid lines approximately coincide with the torque-speed relationship of MotB(Δ72–100) motors obtained in this study (red-filled circles).

higher load than that the wild-type motor responds to dissociate its stators. As toque generation by the motor applies an equal and opposite force on the PG layer through $MotB_C$, we propose that $MotB_C$ may act as a mechano-sensitive structural switch to regulate a load-dependent assembly-disassembly equilibrium of the stators and that an appropriate length of the stalk containing residues 72 to 100 may stabilize this structural switch during the torque generation cycle.

The crystal structure of a *Salmonella* $MotB_C$ fragment corresponding to residues 99 to 276 of MotB has been determined by X-ray crystallography[17] (Fig. 1B). MotB lacking residues 51 to 110 and 271 to 309 exerts the motor function to some degree, indicating that residues 111 to 270 within $MotB_C$ are essential[26]. This $MotB_C$ structure is, however, too small to reach the PG layer if connected directly to MotB-TM, suggesting that unfolding the N-terminal region of $MotB_C$, including two helices α1 and α2 and a strand β1, must occur to make the stalk long enough for the PGB domain to reach the PG layer[17]. The L119P/E mutations in helix α1 of MotB(Δ51–100), which would destabilize the hydrophobic core formed with L149 in strand β2 and V183 and I187 after helix α3 (Fig. 1B), arrest cell growth when overproduced, possibly by opening the proton channel of the MotA/B(Δ51–100) complex even before it is incorporated into the motor to be activated as the stator as well as the proton channel[17,28]. The L119P/E mutations also increase the assembly efficiency of the MotA/B(Δ51–100) complex into the motor[17], indicating that these mutations must alter the conformation of the MotA/B(Δ51–100) complex. Therefore, it is possible that these hydrophobic interactions act as a switch to regulate the assembly and disassembly of the stators and that the stalk formed by residues 51–100 somehow interplays with this structural switch to control the number of active stators in a load dependent manner.

## Materials and Methods

### Bacterial strains, plasmids and media

*Salmonella* strains SJW1103 (wild-type for motility and chemotaxis)[41], SJW2241 (Δ*motA-motB*)[42], MM3076iC [Δ*cheA-cheZ fliC*(Δ204–292)][37] and YSC2123 [Δ*motA-motB* Δ*cheY fliC*(Δ204–292)][7] were used in this study. L-broth (LB) and motility medium (pH 7.0) were prepared as previously described[43].

### DNA manipulations and plasmid construction

DNA manipulations were carried out as described before[44]. To construct pDC01, which encodes MotA and MotB(Δ72–100) on pBAD24[45], QuickChange site-directed mutagenesis was performed as described in the manufacturer's instructions (Stratagene) with a plasmid, pYC20[6], which encodes MotA and MotB on pBAD24, as a template DNA and 5′-TTGGCCACCGCGGTACAGCCGAATATCG ACGAG-3′ and 5′-CTCGTCGATATTCGGCTGTACCGCG GTGGCCAA-3′ as oligonucleotide primers. In-frame deletion of residues 72 to 100 of MotB was confirmed by DNA sequencing. DNA sequencing reactions were carried out using BigDye v3.1 as described in the manufacturer's instructions (Applied Biosystems), and then the reaction mixtures were analyzed by a 3130 Genetic Analyzer (Applied Biosystems).

### Preparation of whole cell proteins and immunoblotting

SJW1103 harboring pBAD24 and SJW2241 transformed with pBAD24 or pDC01 were grown overnight in LB containing 50 μg/ml ampicillin (Amp) with shaking at 30°C. These overnight cultures were inoculated into fresh LB + Amp with 0%, 0.002%, 0.02%, 0.2% arabinose and grown at 30°C for 5 h with shaking. After centrifugation, cell pellets were suspended in a SDS-loading buffer and normalized by cell density to give a constant amount of cells. After sodium dodecyl sulfate-polyacrylamide gel electrophoresis (SDS-PAGE), immunoblotting with polyclonal anti-MotB antibody was carried out as described previously[46].

### Measurements of free-swimming speeds of motile *Salmonella* cells

For measurements of swimming speeds, *Salmonella* cells were observed under a phase contrast microscope (CH40, Olympus) at room temperature. The swimming speed of individual cells was analyzed as described before[43].

### Measurements of the membrane potential and intracellular pH of *Salmonella* cells

The membrane potential was measured as described by Lo *et al*[30]. Overnight cultures of SJW1103 harboring pBAD24 and SJW2241 carrying pBAD24 were inoculated into fresh LB+Amp with 0.2% arabinose and grown at 30°C for 5 h with shaking. These *Salmonella* cells were suspended in motility medium plus 10 mM EDTA for 20 min and then

washed with the motility medium. After centrifugation, the cells were resuspended in the motility medium containing 0.1 μM tetramethyl-rhodamine methyl ester (TMRM) (Invitrogen) and then incubated for 10 min at room temperature. Bacterial cell bodies and epi-fluorescence of TMRM were observed as described before[6]. Calculation of the membrane potential was carried out as described[30] with minor modifications. More than 100 cells of each strain were measured at an external pH value of 7.0.

Intracellular pH measurements with a ratiometric fluorescent pH indicator protein, pHluorin[31], were carried out at an external pH value of 7.0 as described before[28,37].

**Bead assays**

Overnight cultures of MM3076iC carrying pBAD24 and YSC2123 harboring pDC01were diluted 1:100 in fresh LB + Amp and incubated with shaking at 30°C. At an $OD_{600}$ of about 0.8, protein expression was fully induced by adding arabinose, and then the incubation was continued at 30°C for 30 min. The expression level of MotB(Δ72–100) was checked by immunoblotting with polyclonal anti-$MotB_C$ antibody. The cells were passed through a 25G needle to partially shear their sticky flagellar filaments and attached to a cover slip (Matsunami glass). Then, polystyrene beads with diameters of 1 and 0.5 μm (Invitrogen), or a gold nanoparticle with a diameter of 60 nm (BBI) were attached to the filament. Bead images were recorded at 1-ms or 0.9-ms intervals using a high-speed camera (ICL-B0620M-KC, IMPERX) mounted on a dark-field microscope (BX53, U-DCW, Olympus) with a 40× immersion objective lens for the polystyrene beads (UPlanFLN 40×, Olympus) or a 100× oil immersion objective lens for the gold nanoparticle (UPlanFLN 100×, Olympus). To change viscosity of the external motility media, we used Ficoll (PM400, Amersham Biosciences). All measurements were carried out at 23°C. Viscosities of the motility media with or without Ficoll were measured with a viscometer (SV-1A, A&D): 0.97 mPa×s for 0% (motility medium without Ficoll), 1.58 mPa×s for 3% Ficoll, 2.71 mPa×s for 6% Ficoll, 6.76 mPa×s for 12% Ficoll.

Rotation rate, rotation radius and torque were calculated as described previously[9]. The average rotation rate, $<\omega>$, and standard deviation, $\sigma_\omega$, of each rotation data was calculated as follows as described before[32]:

$$\langle \omega \rangle = \frac{N}{\Sigma_{k=1}^{N} \tau(k)} \quad (1)$$

$$\sigma_\omega = \sqrt{\frac{\Sigma_{k=1}^{N} \{\omega(k) - \langle \omega \rangle^2\} \tau(k)}{\Sigma_{k=1}^{N} \tau(k)}} \quad (2)$$

where $N$ is the total number of revolutions, $\tau(k)$ is the rotation period for the $k$th revolution, which is obtained from the peak to peak interval of periodic change in the bead position, and $\omega(k)$ is the rotation rate for the $k$th revolution, which is equal to $1/\tau(k)$.

## Acknowledgements

We thank Seiji Kojima for critical reading of the manuscript and helpful comments. This work was supported in part by JSPS KAKENHI Grant Numbers 24770141 (to S.N.), 24570177 (to S.K.), and 21227006 and 25000013 (to K.N.), and by a Grant-in-Aid for Scientific Research on Innovative Areas "Spying minority in biological phenomena" (23115008 to T.M.) of MEXT, Japan. D.J.C. was a research fellow of the "System Dynamics of Biological Function" Global Centre of Excellence program of Osaka University.

## References

1. Berg, H. C. The rotary motor of bacterial flagella. *Annu. Rev. Biochem.* **72**, 19–54 (2003).
2. Kojima, S. & Blair, D. F. The bacterial flagellar motor: structure and function of a complex molecular machine. *Int. Rev. Cytol.* **233**, 93–134 (2004).
3. Minamino, T., Imada, K. & Namba, K. Molecular motors of the bacterial flagella. *Curr. Opin. Struct. Biol.* **18**, 693–701 (2008).
4. Sowa, Y. & Berry, R. M. Bacterial flagellar motor. *Q Rev. Biophys.* **41**, 103–132 (2008).
5. Zhou, J., Lloyd, S. A. & Blair, D. F. Electrostatic interactions between rotor and stator in the bacterial flagellar motor. *Proc. Natl. Acad. Sci. USA* **95**, 6436–6441 (1998).
6. Morimoto, Y. V., Nakamura, S., Kami-ike, N., Namba, K. & Minamino, T. Charged residues in the cytoplasmic loop of MotA are required for stator assembly into the bacterial flagellar motor. *Mol. Microbiol.* **78**, 1117–1129 (2010).
7. Morimoto, Y. V., Nakamura, S., Hiraoka, K. D., Namba, K. & Minamino, T. Distinct roles of highly conserved charged residues at the MotA-FliG interface in bacterial flagellar motor rotation. *J. Bacteriol.* **195**, 474–481 (2013).
8. Braun, T. F., Al-Mawasawi, L. Q., Kojima, S. & Blair, D. F. Arrangement of core membrane segments in the MotA/MotB protein-channel complex of *Escherichia coli*. *Biochemistry* **43**, 35–45 (2004).
9. Che, Y-S., Nakamura, S., Kojima S., Kami-ike, N., Namba, K. & Minamino, T. Suppressor analysis of the MotB(D33E) mutation to probe the bacterial flagellar motor dynamics coupled with proton translocation. *J. Bacteriol.* **190**, 6660–6667 (2008).
10. Kim, E. A., Price-Carter, M., Carlquist, W. C. & Blair, D. F. Membrane segment organization in the stator complex of the flagellar motor: implications for proton flow and proton-induced conformational change. *Biochemistry* **47**, 11332–11339 (2008).
11. Zhou, J., Sharp, L. L., Tang, H. L., Lloyd, S. A. & Blair, D. F. Function of protonatable residues in the flagellar motor of *Escherichia coli*: a critical role for Asp32 of MotB. *J. Bacteriol.* **180**, 2729–2735 (1998).
12. Kojima, S. & Blair, D. F. Conformational change in the stator of the bacterial flagellar motor. *Biochemistry* **40**, 13041–13050 (2001).
13. Nakamura, S., Morimoto, Y. V., Kami-ike, N., Minamino, T. & Namba, K. Role of a conserved prolyl residue (Pro-173) of MotA in the mechanochemical reaction cycle of the proton-driven flagellar motor of *Salmonella*. *J. Mol. Biol.* **393**, 300–307 (2009).
14. Kojima, S., Furukawa, Y., Matsunami, H., Minamino, T. & Namba, K. Characterization of the periplasmic domain of

MotB and implications for its role in the stator assembly of the bacterial flagellar motor. *J. Bacteriol.* **190**, 3314–3322 (2008).
15. De Mot, R. & Vanderleyden, J. The C-terminal sequence conservation between OmpA-related outer membrane proteins and MotB suggests a common function in both gram-positive and gram-negative bacteria, possibly in the interaction of these domains with peptidoglycan. *Mol. Microbiol.* **12**, 333–334 (1994).
16. Roujeinikova, A. Crystal structure of the cell wall anchor domain of MotB, a stator component of the bacterial flagellar motor: implications for peptidoglycan recognition. *Proc. Natl. Acad. Sci. USA* **105**, 10348–10353 (2008).
17. Kojima, S., Imada, K., Sakuma, M., Sudo, Y., Kojima, C., Minamino, T., Homma, M. & Namba, K. Stator assembly and activation mechanism of the flagellar motor by the periplasmic region of MotB. *Mol. Microbiol.* **73**, 710–718 (2009).
18. Blair, D. F., Kim, D. Y. & Berg, H. C. Mutant MotB proteins in *Escherichia coli*. *J. Bacteriol.* **173**, 4049–4055 (1991).
19. Garza, A. G., Biran, R., Wohlschlegel, J. A. & Manson, M. D. Mutations in *motB* suppressible by changes in stator or rotor components of the bacterial flagellar motor. *J. Mol. Biol.* **258**, 270–285 (1996).
20. Block, S. M. & Berg, H. C. Successive incorporation of force-generating units in the bacterial rotary motor. *Nature* **309**, 470–472 (1984).
21. Blair, D. F. & Berg, H. C. Restoration of torque in defective flagellar motors. *Science* **242**, 1678–1681 (1988).
22. Leake, M. C., Chandler, J. H., Wadhams, G. H., Bai, F., Berry, R. M. & Armitage, J. P. Stoichiometry and turnover in single, functioning membrane protein complexes. *Nature* **443**, 355–358 (2006).
23. Lele, P. P., Hosu, B. G. & Berg, H. C. Dynamics of mechanosensing in the bacterial flagellar motor. *Proc. Natl. Acad. Sci. USA* **110**, 11839–11844 (2013).
24. Tipping, M. J., Delalez, N. J., Lim, R., Berry, R. M. & Armitage, J. P. Load-dependent assembly of the bacterial flagellar motor. *MBio* **4**, e00551-13 (2013).
25. Che, Y. S., Nakamura, S., Morimoto, Y. V., Kami-ike, N., Namba, K. & Minamino, T. Load-sensitive coupling of proton translocation and torque generation in the bacterial flagellar motor. *Mol. Microbiol.* DOI: 10.1111/mmi.12453 (2013).
26. Muramoto, K. & Macnab, R. M. Deletion analysis of MotA and MotB, components of the force-generating unit in the flagellar motor of *Salmonella*. *Mol. Microbiol.* **29**, 1191–1202 (1998).
27. Hosking, E. R., Vogt, C., Bakker, E. P. & Manson, M. D. The *Escherichia coli* MotAB proton channel unplugged. *J. Mol. Biol.* 364, 921–937 (2006).
28. Morimoto, Y. V., Che, Y-.S., Minamino, T. & Namba, K. Proton-conductivity assay of plugged and unplugged MotA/B proton channel by cytoplasmic pHluorin expressed in *Salmonella*. *FEBS lett.* **584**, 1268–1272 (2010).
29. Gabel, C. V. & Berg, H. C. The speed of the flagellar rotary motor of *Escherichia coli* varies linearly with protonmotive force. *Proc. Natl. Acad. Sci. USA* **100**, 8748–8751 (2003).
30. Lo, C. J., Leake, M. C., Pilizota, T. & Beryy, R. M. Non-equivalence of membrane voltage and ion-gradient as driving forces for the bacterial flagellar motor at low load. *Biophys. J.* **93**, 294–302 (2007).
31. Miesenbock, G., Angelis, D. A. D. & Rothman, J. E. Visualizing secretion and synaptic transmission with pH-sensitive green fluorescent proteins. *Nature* **394**, 192–195 (1998).
32. Muramoto, K., Magariyama, Y., Homma, M., Kawagishi, I., Sugiyama, S., Imae, Y. & Kudo, S. Rotational fluctuation of the sodium-driven flagellar motor of *Vibrio alginolyticus* induced by binding of inhibitors. *J. Mol. Biol.* **259**, 687–695 (1996).
33. Chen, X. & Berg, H. C. Torque-speed relationship of the flagellar motor of *Escherichia coli*. *Biophys. J.* **78**, 1036–1041 (2000).
34. Chen, X. & Berg, H. C. Solvent-isotope and pH effects on flagellar rotation in *Escherichia coli*. *Biophys. J.* **78**, 2280–2284 (2000).
35. Sowa, Y., Hotta, H., Homma, M. & Ishijima, A. Torque-speed relationship of the $Na^+$-driven flagellar motor of Vibrio alginolyticus. *J. Mol. Biol.* **327**, 1043–1051 (2003).
36. Inoue, Y., Lo, C. J., Fukuoka, H., Takahashi, H., Sowa, Y., Pilizota, T., Wadhams, G. H., Homma, M., Berry, R. M. & Ishijima, A. Torque-speed relationships of $Na^+$-driven chimeric flagellar motors in *Escherichia coli*. *J. Mol. Biol.* **376**, 1251–1259 (2008).
37. Nakamura, S., Kami-ike, N., Yokota, P. J., Kudo, S., Minamino, T. & Namba, K. Effect of intracellular pH on the torque-speed relationship of bacterial proton-driven flagellar motor. *J. Mol. Biol.* **386**, 332–338 (2009).
38. Ryu, W. S., Berry, R. M. & Berg, H. C. Torque-generating units of the flagellar motor of *Escherichia coli* have a high duty ratio. *Nature* **403**, 444–447 (2000).
39. Yuan, J. & Berg, H. C. Resurrection of the flagellar rotary motor near zero load. *Proc. Natl. Acad. Sci. USA* **105**, 1182–1185 (2008).
40. Reid, S. W., Leake, M. C., Chandler, J. H., Lo, C. J., Armitage, J. P. & Berry, R. M. The maximum number of torque-generating units in the flagellar motor of *Escherichia coli* is at least 11. *Proc. Natl. Acad. Sci. USA* **103**, 8066–8071 (2006).
41. Yamaguchi, S., Fujita, H., Sugata, K., Taira, T. & Iino, T. Genetic analysis of H2, the structural gene for phase-2 flagellin in *Salmonella*. *J. Gen. Microbiol.* **130**, 255–265 (1984).
42. Komoriya, K., Shibano, N., Higano, T., Azuma, N., Yamaguchi, S. & Aizawa, S. Flagellar proteins and type III-exported virulence factors are the predominant proteins secreted into the culture media of *Salmonella typhimurium*. *Mol. Microbiol.* **34**, 767–779 (1999).
43. Minamino, T., Imae, Y., Oosawa, F., Kobayashi, Y. & Oosawa, K. Effect of intracellular pH on the rotational speed of bacterial flagellar motors. *J. Bacteriol.* **185**, 1190–1194 (2003).
44. Saijo-Hamano, Y., Minamino, T., Macnab, R. M. & Namba, K. Structural and functional analysis of the C-terminal cytoplasmic domain of FlhA, an integral membrane component of the type III flagellar protein export apparatus in *Salmonella*. *J. Mol. Biol.* **343**, 457–466 (2004).
45. Guzman, L. M., Belin, D., Carson, M. J. & Beckwith, J. Tight regulation, modulation, and high-level expression by vectors containing the arabinose PBAD promoter. *J. Bacteriol*. **177**, 4121–4130 (1995).
46. Minamino, T. & Macnab, R. M. Components of the *Salmonella* flagellar export apparatus and classification of export substrates. *J. Bacteriol.* **181**, 1388–1394 (1999).